On the Viability for *s*-process nucleosynthesis in low metallicity massive binaries

BRANDON L. BARKER [ID][1, 2, 3, 4, 5, *] AND MATHIEU RENZO [ID][6]

[1]*Department of Physics and Astronomy, Michigan State University, East Lansing, MI 48824, USA*
[2]*Department of Computational Mathematics, Science, and Engineering, Michigan State University, East Lansing, MI 48824, USA*
[3]*Computational Physics and Methods, Los Alamos National Laboratory, Los Alamos, NM 87545, USA*
[4]*Center for Nonlinear Studies, Los Alamos National Laboratory, Los Alamos, NM 87545, USA*
[5]*Center for Theoretical Astrophysics, Los Alamos National Laboratory, Los Alamos, NM 87545, USA*
[6]*Center for Computational Astrophysics, Flatiron Institute, New York, NY 10010, USA*

ABSTRACT

The *s*-process is responsible for the synthesis of roughly half of the elements heavier than ^{56}Fe. The primary astrophysical site of the *s*-process is asymptotic giant branch (AGB) stars. However, observations of metal-poor ultra-faint dwarf galaxies show an *s*-process enrichment on timescales too short to be explained by AGB stars. Rapid rotation in low metallicity massive stars has been shown to allow for an enhanced weak *s*-process capable of producing nuclei up to mass number $A \sim 90$. Rotationally induced mixing during core He-burning leads to an enhancement of ^{22}Ne which serves as the neutron source for the *s*-process through ^{22}Ne(α,n)^{25}Mg. This channel operates in rapidly rotating massive stars which are, however, rare. A much more natural, and common, source of rapid rotation is binary interaction. Case B mass transfer will result in a sufficient spin up of the core to produce an *s*-process. We use the open source stellar evolutionary code MESA to produce a grid of binary stellar models. We show that these models produce ^{22}Ne comparable to the rapidly rotating single star evolutionary models, making them a viable astrophysical site for the *s*-process. This site is potentially much more common than rapidly rotating massive single stars and likely has numerous consequences for galactic chemical evolution.

1. INTRODUCTION

The slow neutron capture process, or *s*-process, is responsible for roughly half of the elements heavier than ^{56}Fe (Burbidge et al. 1957; Seeger et al. 1965; Käppeler et al. 2011). Through sequences of (n,γ) neutron captures and β-decays heavy elements may be formed. The *s*-process occurs in environments with a sufficient neutron flux and population of seed nuclei, typically ^{56}Fe. It is distinct from the rapid neutron capture process in that the timescale for neutron capture is slower than the timescale for β-decay leading to a nucleosynthesis path close to the valley of stability. It is further divided into the weak and main *s*-process, with the weak process being responsible being responsible for nuclei up to mass number $A \approx 90$. The weak *s*-process is believed to primarily occur in massive stars ($\gtrsim 10 \ \mathrm{M_\odot}$) (Prantzos et al. 1990; Pignatari et al. 2010) which will end their lives with a core-collapse event (Bethe 1990; Mezzacappa 2001, 2005, 2023; Mezzacappa et al. 2020; Janka 2012; Janka et al. 2016;

Burrows 2013; Burrows & Vartanyan 2021; Hix et al. 2014; Müller et al. 2016; Müller 2020; Couch 2017; Pejcha 2020). The main *s*-process occurs in low mass, asymptotic giant branch stars (Iben 1983; Kappeler et al. 1989; Käppeler et al. 2011; Bisterzo et al. 2015, and references therein).

The weak *s*-process occurs during the He-core burning phase of of stellar evolution. During this stage, ^{14}N produced in the H-burning shell may be engulfed into the He-burning core. Here, the mixed ^{14}N may produce ^{22}Ne through a mix of α-captures and β-decays ^{14}N(α,γ)^{18}F(e^-, ν_e) ^{18}O(α,γ)^{22}Ne. This ^{22}Ne in turn sets the stage for the weak *s*-process: the ^{22}Ne(α,n)^{25}Mg reaction provides the neutron source necessary for subsequent neutron captures. This is the classical picture of the weak *s*-process: production of ^{14}N in the H-burning shell provides the means for ^{22}Ne to be formed in the He-burning core, which in turn acts as a neutron source. This picture, however, is sensitive to the stellar rotational profile, as rotationally induced mixing between the He-burning core and H-burning shell can enhance ^{14}N production and, consequently, enhance ^{22}Ne production and the strength of the neutron source. This enhancement is most prominent at low metallicities (e.g., Frischknecht et al. 2016) where the combined effects of compactness and reduced an-

Corresponding author: Brandon L. Barker
barker49@msu.edu

[*] NSF Graduate Research Fellow

gular momentum loss through winds results in more rapidly rotating stellar profiles and enhanced rotational mixing.

Observations of low metallicity environments, such as ultra-faint dwarf galaxies (e.g., Tarumi et al. 2021) necessitate the existence of a prompt *s*-process source, taken to be the weak *s*-process. The weak *s*-process is typically explained through rapidly rotating, massive, low metallicity single stars. The rapid rotation at low metallicity provides the rotationally induced mixing to support a robust ^{22}Ne production. However, such rapid rotation rates for single stars is uncommon.

An alternative, historically overlooked potential production site that naturally supplies the needed rotation is binary evolution. During mass transfer, the accretor star spins up to near or even critical rotation. At low metallicity, where little angular momentum can be carried away through winds, this results in a significant spin up of the core. For Case B mass transfer, where the accretor is still on its main sequence, this could result in a rapidly rotating core during central helium burning, fueling rotational mixing and supporting a weak *s*-process.

In this work, we pursue a proof of concept calculation exploring the prospects for *s*-process nucleosynthesis in massive binary accretors. Taking a low metallicity, massive binary as our example, we demonstrate that rotational mixing induced after mass transfer provides the necessary environment for *s*-process nucleosynthesis. In Section 2 we describe the stellar evolutionary models used in this work. In Section 3 we describe the nucleosynthetic properties of the models. Finally, in Section 4 we summarize the results and lay out future plans.

2. STELLAR EVOLUTIONARY MODELS

We follow the coupled evolution of a pair of massive stars in a binary system using MESA (version 15140 Paxton et al. 2011, 2013, 2015, 2018, 2019) for systems which experience mass transfer after the donor's main sequence (so-called case B mass transfer). Evolution with MESA is followed through mass transfer until central ^{4}He depletion in the accretor. Unless otherwise noted, we follow the numerical setup described in (Renzo et al. 2023). We take solar metallicity to be $Z = 0.019$. We summarize here some key parameter choices, and explore variations of some in Section 3.1.

We use the Ledoux criterion for convective stability with a mixing length parameter of 1.5. Semiconvection and thermohaline mixing are included. Rotation is treated in the commonly used shellular approximation and we assume tidal synchronization with rigid body rotational at the beginning of our simulations. We treat mixing due to meridional currents diffusively. We include also secular and dynamical shear instabilities. Transport of angular momentum is treated following the Spruit-Tayler dynamo following Heger et al. (2000).
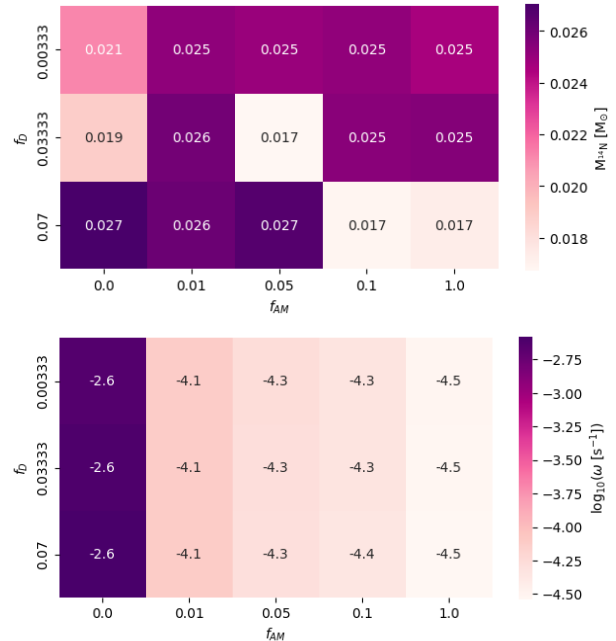

Figure 1. Mass of synthesized ^{14}N in the He burning region (top) and angular velocity in the He burning region (bottom) at He depletion for our grid of models.

The shellular approximation for rotation breaks down as rotation approaches critical rates. To keep rotation sub-critical, we enhance the wind mass loss rate, and hence angular momentum transport away from the star, when the rotation rate is with 95% of critical.

Stellar winds are implemented following Vink et al. (2001) for hot regions (T > 11000K). Cool regions (T < 10000K) follow de Jager et al. (1988) with linear interpolation between these regions.

For simplicity, we assume that the binary is detached following the mass transfer episode. We follow the evolution of the accretor as an isolated star until it reaches central ^{4}He depletion. By detaching the binary we greatly reduce the computational complexity by losing potential, but not expected, mass transfer episodes. We also neglect post RLOF tides and interactions with the donor's supernova ejecta.

3. RESULTS

3.1. *Single Stars*

We begin by exploring a grid of low metallicity, single star evolutionary models. We seek to find the parameters that best reproduce Chieffi & Limongi (2013) and use these values to guide the later binary stellar evolutionary models. Following Chieffi & Limongi (2013), we take $Z = 0.001345$. These models are initialized with 300 km s^{-1} rotation rates. We vary am_D_mix_factor and am_nu_factor (henceforth f_D and f_{AM}) which scale chemical mixing and angular momentum transport, respectively. In the grid of mod-
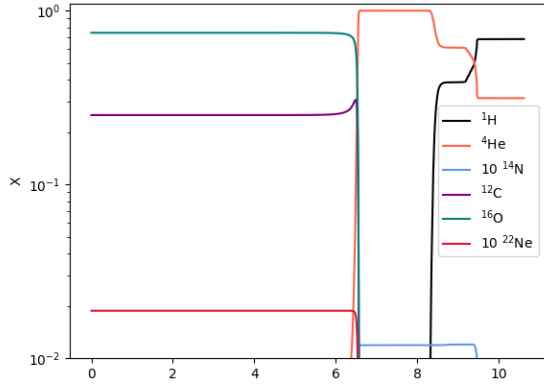
Figure 2. Mass fractions for the $17\mathrm{M}_\odot$ single star model.
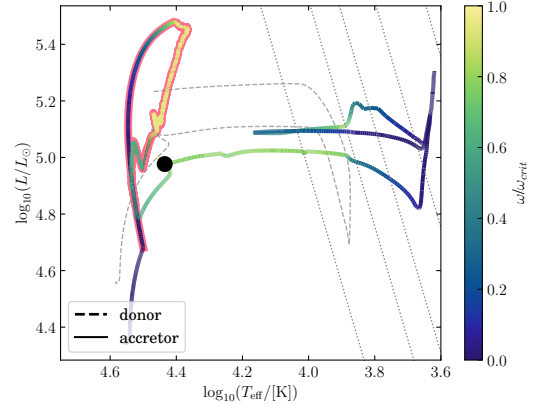

Figure 3. HR diagram of the binary system. The evolution of the donor star until RLOF detachment is shown in grey, dashed lines. The accretor is shown in solid lines colored by the fraction of critical rotation until core helium depletion through RLOF (marked by a pink outline). Thin dotted lines mark tracks of constant radii of $R = 100, 200, 300, 500, 1000\,\mathrm{R}_\odot$.

els we take $f_{AM} = \{0.0, 0.01, 0.05, 0.1, 1.0\}$ and $f_D = \{0.003333, 0.03333, 0.07\}$. $f_{AM} = 0.0$ corresponds to perfect angular momentum conservation and serves as a limiting case. Much larger values of f_D tended to overly mix the stellar structure and resulted in chemically homogeneous evolution, so 0.07 serves as our upper bound. Furthermore, we take `am_gradmu_factor`, f_μ, to be 0.03. $f_\mu = 0.03$ and $f_D = 0.07$ correspond to the values of f_μ and f_c reported in Chieffi & Limongi (2013) using the `FRANEC` code for their diffusive angular momentum transport scheme. In Figure 1 we show the mass of synthesized ^{14}N (top) and angular velocity (bottom) in the He burning region for the grid of models. Overall, we see the expected behavior: increasing the mixing efficiency tends to increase production of ^{14}N, although the behavior isn't monotonic. Similarly, increasing the angular momentum transport efficiency further spins down the core and inhibits rotational mixing. Given these results, in the following we take $f_D = 0.03333$ and $f_{AM} = 1.0$ – the default values – as they allow for nearly maximal masses of synthesized ^{14}N. While some values give slightly larger masses, the differences are small enough to be within numerical noise.

For the sake of comparison with later binary stellar evolution models, we follow the single star evolution of a low metallicity ($Z = 0.0019$), rapidly rotating (initial surface rotation of $300\,\mathrm{km\,s^{-1}}$), $17\mathrm{M}_\odot$ model to central ^{4}He depletion. In Figure 2 we show the relevant compositional profiles profiles for the single star comparison model.

3.2. *Binary Stars*

Motivated by the results of the previous section, we run a selection of binary models. We follow the evolution through the mass transfer episode, detach the binary, and follow the evolution of the accretor until central ^{4}He depletion. We select models with parameters $(\mathrm{M}_1, \mathrm{M}_2, P, Z) = (20,17,100,Z_\odot/10)$, $(18,15,100,Z_\odot/10)$,

$(20,17,100,Z_\odot/100)$. These initial masses and orbital periods are chosen to ensure Case B mass transfer and for numerical convergence. The low metallicities are chosen to sample the low metallicity environments typical of, e.g., ultra-faint dwarf galaxies where early *s*-process enrichment is observed. In Figure 3 we show an example Hertzsprung-Russell (HR) diagram, in this case for the $(20,17,100,Z_\odot/10)$ model. The HR track for the accretor is shown in solid lines colored by rotation rate scaled to critical rotation. The evolution of the donor, until detachment, is shown in grey, dashed lines. The HR track during the mass transfer episode is outlined in pink.

In Figures 4 and 5 we show relevant mass fractions up to ^{22}Ne (top) and rotational and diffusion profiles (bottom) for the two tenth of solar metallicity models $(20,17,100,Z_\odot/10)$ and $(18,15,100,Z_\odot/10)$. In both cases we see the development of a population of ^{22}Ne within the core. We estimate the mass of ^{22}Ne produced that might possibly be ejected, taking this as a proxy for the possible robustness of the *s*-process. This proxy is necessary in the absence of an extensive nuclear reaction network capable of following the *s*-process. We estimate the mass of ^{22}Ne outside $1.4\mathrm{M}_\odot$, taking this value as a naive estimate of the neutron star mass to be formed after core-collapse, assuming anything outside of this mass to be ejected as future *s*-process enriched material. For the $17\mathrm{M}_\odot$ and $15\mathrm{M}_\odot$ accretors we see the production of $0.009\mathrm{M}_\odot$ and $0.007\mathrm{M}_\odot$ of ^{22}Ne, respectively. For comparison, the rapidly rotating $17\mathrm{M}_\odot$ single star model of Section 3.1 (Figure 2) produces approximately $0.009\mathrm{M}_\odot$ of ^{22}Ne, identical to the binary accretor of the same zero-age main sequence (ZAMS) mass. We conclude that, at this metallicity and for a selec-
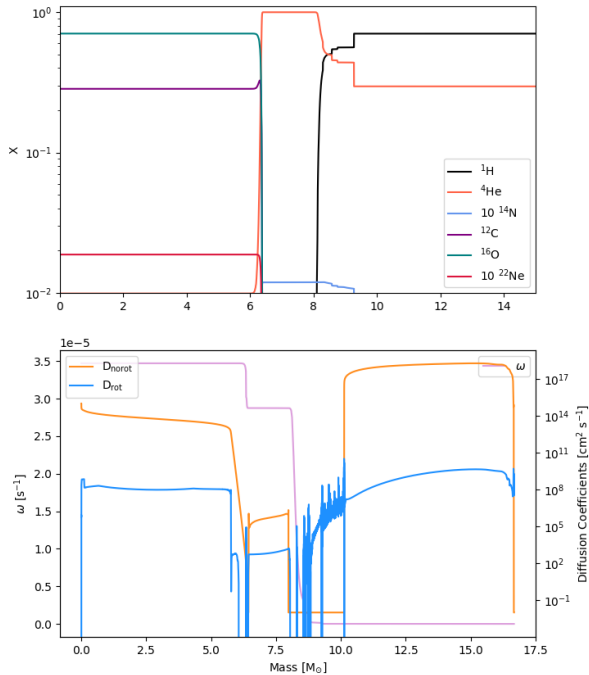
Figure 4. Mass fractions and diffusion coefficients for model $(20,17,100,Z_\odot/10)$. Top: Compositional profiles for the ^{1}H (black), ^{4}He (orange), ^{14}N (blue; scaled up by a factor of 10), ^{12}C (purple), ^{16}O (teal), and ^{22}Ne (red; scaled up by a factor of 10) mass fractions. Bottom: Rotational profile (left axis; pink) and diffusion coefficients, separated into rotational (blue) and non-rotational (yellow) components (right axis).

Figure 5. The same as Figure 4 but for model $(18,15,100,Z_\odot/10)$

tion of binary parameters at least, that binary accretors are an equivalently efficient producer of *s*-process nuclei.

Next, we turn to the lowest metallicity model, $(20,17,100,Z_\odot/100)$. At present we have only one model for $Z = Z_\odot/100$ due to numerical difficulties associated with the excessively high rotation rates and, equivalently, low mass loss rates. In Figure 6 we show the compositional profiles (top) and rotational and diffusion profiles (bottom). In contrast to the tenth-of-solar metallicity models, this model struggles to produce a a population of ^{22}Ne in its core. Indeed, at an order of magnitude lower metallicity we see approximately an order of magnitude reduction in synthesized ^{22}Ne, producing about $0.0009\mathrm{M_\odot}$.

4. DISCUSSION AND CONCLUSIONS

In this exploratory work we have explored the prospects for weak *s*-process nucleosynthesis, typically attributed to rapidly rotating massive stars, in massive binary accretors. We carefully select binary stellar evolutionary models, with corresponding single star stellar evolutionary models, to
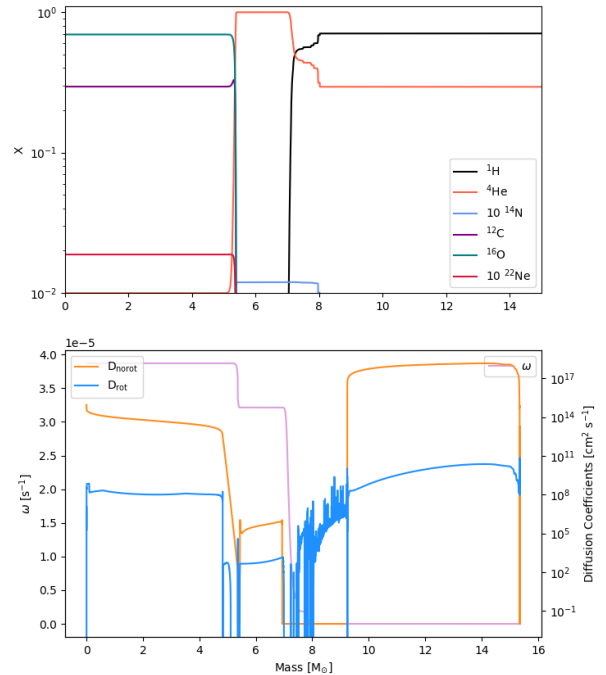
probe *s*-process nucleosynthesis in low metallicity environments. Taking the mass of synthesized ^{22}Ne as a proxy for potential *s*-process nucleosynthesis, we have demonstrated that binary accretors are a viable source of *s*-process nucleosynthesis.

We begin by computing a grid of single star stellar evolutionary models, computed with MESA, to explore the sensitivity of mixing between the helium core and hydrogen shell during core helium burning to angular momentum transport. Using the mass of synthesized ^{14}N during core helium burning as an indicator of mixing, we find comparable results to previous works (e.g., Chieffi & Limongi 2013).

Using the results of this mixing parameter study as a starting point, we compute a selection of binary stellar evolutionary models which undergo a mass transfer episode during the accretor's main sequence (so-called Case B mass transfer). To adequately probe prospects in low metallicity environments, we compute both $Z = 0.0019$ and $Z = 0.00019$ models – approximately one tenth and one hundredth of solar. We assume initial orbital periods of 100 days and tidal synchronization and compute models with $(M_1, M_2) = (20\mathrm{M_\odot}, 17\mathrm{M_\odot})$ and $(18\mathrm{M_\odot}, 15\mathrm{M_\odot})$ at one tenth of solar and the latter at one hundredth of solar. In both tenth-of-solar binary evolutionary models, the accretor is shown to experience an enhancement of ^{22}Ne comparable to rapidly rotating
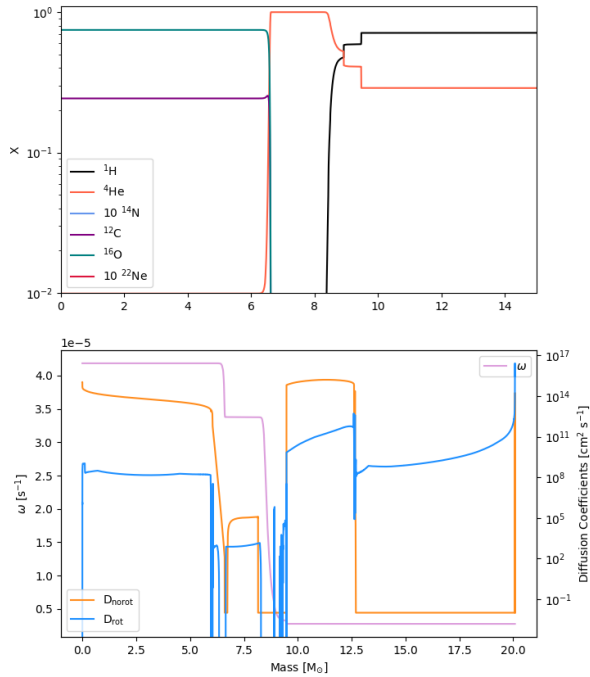
The preliminary results here show that massive binary accretors are a viable, and as of yet unexplored, site for the weak *s*-process. Further work will be necessary to determine the universality of this site. Building off of these preliminary results, we will expand our set of binary stellar evolutionary models to be a grid that sufficiently samples donor mass, accretor mass, orbital period, and metallicity, including extensions to solar metallicity. Such a grid will allow us to determine where, and to what extent, this new nucleosynthesis site operates. Furthermore, in the current work we took the presence ^{22}Ne as a tracer for *s*-process potential. Future work will include larger reaction networks, and potentially artificially driven core-collapse supernovae, to determine the exact *s*-process yields from these models. These yields used in union with population synthesis results will allow us to place constraints on the role which massive binary accretors play in galactic chemical evolution.

Software: NumPy (Harris et al. 2020), SciPy (Jones et al. 2001), MESA (version 15140 Paxton et al. 2011, 2013, 2015, 2018, 2019)

Figure 6. The same as Figure 5 but for model $(18,15,100,Z_\odot/100)$

single stars. The lower metallicity model fails to produce an appreciable mass of synthesized ^{22}Ne.

REFERENCES

Bethe, H. A. 1990, Reviews of Modern Physics, 62, 801, doi: 10.1103/RevModPhys.62.801

Bisterzo, S., Gallino, R., Käppeler, F., et al. 2015, MNRAS, 449, 506, doi: 10.1093/mnras/stv271

Burbidge, E. M., Burbidge, G. R., Fowler, W. A., & Hoyle, F. 1957, Reviews of Modern Physics, 29, 547, doi: 10.1103/RevModPhys.29.547

Burrows, A. 2013, Reviews of Modern Physics, 85, 245, doi: 10.1103/RevModPhys.85.245

Burrows, A., & Vartanyan, D. 2021, Nature, 589, 29, doi: 10.1038/s41586-020-03059-w

Chieffi, A., & Limongi, M. 2013, ApJ, 764, 21, doi: 10.1088/0004-637X/764/1/21

Couch, S. M. 2017, Philosophical Transactions of the Royal Society of London Series A, 375, 20160271, doi: 10.1098/rsta.2016.0271

de Jager, C., Nieuwenhuijzen, H., & van der Hucht, K. A. 1988, A&AS, 72, 259

Frischknecht, U., Hirschi, R., Pignatari, M., et al. 2016, MNRAS, 456, 1803, doi: 10.1093/mnras/stv2723

Harris, C. R., Millman, K. J., van der Walt, S. J., et al. 2020, Nature, 585, 357, doi: 10.1038/s41586-020-2649-2

Heger, A., Langer, N., & Woosley, S. E. 2000, ApJ, 528, 368, doi: 10.1086/308158

Hix, W. R., Lentz, E. J., Endeve, E., et al. 2014, AIP Advances, 4, 041013, doi: 10.1063/1.4870009

Iben, I., J. 1983, ApJL, 275, L65, doi: 10.1086/184172

Janka, H.-T. 2012, Annual Review of Nuclear and Particle Science, 62, 407, doi: 10.1146/annurev-nucl-102711-094901

Janka, H.-T., Melson, T., & Summa, A. 2016, Annual Review of Nuclear and Particle Science, 66, 341, doi: 10.1146/annurev-nucl-102115-044747

Jones, E., Oliphant, T., Peterson, P., et al. 2001, SciPy: Open source scientific tools for Python. http://www.scipy.org/

Kappeler, F., Beer, H., & Wisshak, K. 1989, Reports on Progress in Physics, 52, 945, doi: 10.1088/0034-4885/52/8/002

Käppeler, F., Gallino, R., Bisterzo, S., & Aoki, W. 2011, Reviews of Modern Physics, 83, 157, doi: 10.1103/RevModPhys.83.157

Mezzacappa, A. 2001, NuPhA, 688, 158, doi: 10.1016/S0375-9474(01)00690-X

—. 2005, Annual Review of Nuclear and Particle Science, 55, 467, doi: 10.1146/annurev.nucl.55.090704.151608

Mezzacappa, A. 2023, in The Predictive Power of Computational Astrophysics as a Discover Tool, ed. D. Bisikalo, D. Wiebe, & C. Boily, Vol. 362, 215–227, doi: 10.1017/S1743921322001831. https://ui.adsabs.harvard.edu/abs/2023IAUS..362..215M

Mezzacappa, A., Marronetti, P., Landfield, R. E., et al. 2020, arXiv e-prints, arXiv:2007.15099. https://arxiv.org/abs/2007.15099

Müller, B. 2020, Living Reviews in Computational Astrophysics, 6, 3, doi: 10.1007/s41115-020-0008-5

Müller, B., Heger, A., Liptai, D., & Cameron, J. B. 2016, MNRAS, 460, 742, doi: 10.1093/mnras/stw1083

Paxton, B., Bildsten, L., Dotter, A., et al. 2011, ApJS, 192, 3, doi: 10.1088/0067-0049/192/1/3

Paxton, B., Cantiello, M., Arras, P., et al. 2013, ApJS, 208, 4, doi: 10.1088/0067-0049/208/1/4

Paxton, B., Marchant, P., Schwab, J., et al. 2015, ApJS, 220, 15, doi: 10.1088/0067-0049/220/1/15

Paxton, B., Schwab, J., Bauer, E. B., et al. 2018, ApJS, 234, 34, doi: 10.3847/1538-4365/aaa5a8

Paxton, B., Smolec, R., Schwab, J., et al. 2019, ApJS, 243, 10, doi: 10.3847/1538-4365/ab2241

Pejcha, O. 2020, The Explosion Mechanism of Core-Collapse Supernovae and Its Observational Signatures, 189–211

Pignatari, M., Gallino, R., Heil, M., et al. 2010, ApJ, 710, 1557, doi: 10.1088/0004-637X/710/2/1557

Prantzos, N., Hashimoto, M., & Nomoto, K. 1990, A&A, 234, 211

Renzo, M., Zapartas, E., Justham, S., et al. 2023, ApJL, 942, L32, doi: 10.3847/2041-8213/aca4d3

Seeger, P. A., Fowler, W. A., & Clayton, D. D. 1965, ApJS, 11, 121, doi: 10.1086/190111

Tarumi, Y., Suda, T., van de Voort, F., et al. 2021, MNRAS, 505, 3755, doi: 10.1093/mnras/stab1487

Vink, J. S., de Koter, A., & Lamers, H. J. G. L. M. 2001, A&A, 369, 574, doi: 10.1051/0004-6361:20010127